Supporting Information

A Molecular Simulation Study into the Stability of Hydrated Graphene Nanochannels used in Nanofluidics Devices

Christopher D. Williams*, Zixuan Wei, Mohd Rafie bin Shaharudin and Paola Carbone

Department of Chemical Engineering and Analytical Science, School of Engineering, The University of Manchester, Manchester, United Kingdom.

Corresponding Author

*Email: christopher.williams@manchester.ac.uk

paola.carbone@manchester.ac.uk

1. Additional Simulation Details

The graphene sheets in the nanochannel assembly had the atomistic hexagonal lattice structure of graphene with a C-C bond length of 0.1418 nm. In the graphite slabs each sheet consisted of 36660 atoms and in the graphene spacers the sheets consisted of 4980 atoms. Graphene layers were initially stacked in an A-A arrangement, although relaxation by simulation permits the sheets to deviate from this initial stacking arrangement. Carbon atoms at the edge of the spacers in the x-direction were terminated with hydrogens to maintain the correct stoichiometry. The length of the simulation cell in the z-direction, L_z, was set to 12 nm, sufficient to provide a vacuum gap of at least 4 nm, preventing interactions between the bottom and top graphite slabs through the periodic boundary.

Classical MD simulations were performed for both dry and hydrated as well as both rigid and flexible nanochannels. Non-bonded interactions were computed as the sum of electrostatic and vdWs contributions. The latter were evaluated using the Lennard-Jones 12-6 pair potential, $u(r_{ij})$

$$u(r_{ij}) = 4\varepsilon_{ij}\left[\left(\frac{\sigma_{ij}}{r_{ij}}\right)^{12} - \left(\frac{\sigma_{ij}}{r_{ij}}\right)^{6}\right] \quad (S1)$$

where r_{ij} is the distance between atoms i and j and ε_{ij} and σ_{ij} are the energy and distance parameters. Water was usually modelled using the rigid, non-polarisable four-site TIP4P/2005 model (ε_O = 0.77490 kJ mol^{-1} and σ_O = 0.31589 nm). [1] The parameters for carbon atoms in graphene were taken from the Amber potential (ε_C = 0.35982 kJ mol^{-1} and σ_C = 0.33997 nm). [2] The carbon-oxygen cross terms, obtained from the Lorentz-Berthelot combining rules, are ε_{CO} = 0.5280 kJ mol^{-1} and σ_{CO} = 0.3279 nm. Bonded interactions (bond stretching, angle bending and dihedral angle torsions) were also evaluated using the Amber potential.[2] Charges on the hydrogen and carbon atoms terminating the graphene spacers at the edge of the nanochannel were set to +0.158 and −0.158, respectively. [3]

In all simulations, including those with flexible graphite slabs, the n graphene spacers were held rigid, to prevent displacement of the nanochannel in the x-direction during the simulation. After an initial 100 ps equilibration simulations, 5 ns production simulations were performed, from which the output data was collected for post-simulation analysis. Equations of motion were integrated using a timestep of 1 fs. The Verlet cut-off scheme was used to generate the neighbour list. [4] All simulations were performed in the canonical ensemble with a temperature of 298 K maintained using the Nose-Hoover thermostat and a temperature fluctuation period of 2.0 ps. [5, 6] The geometry of water molecules was constrained using the SETTLE algorithm. [7] $u(r_{ij})$ was initially truncated smoothly to zero at the cut-off radius, r_{cut}

= 1.2 nm, using a switch function from r_{cut} − 0.3 nm. Electrostatic interactions were evaluated using the particle-mesh Ewald summation [8] with a real space cut-off matching the vdW cut-off, a Fourier spacing of 0.12 nm and cubic interpolation. However, the sensitivity of the results to cut-off distance was investigated. MD simulations were performed using Gromacs, version 2018.4. [9]

2. Channel Filling Simulations

Two different approaches to obtain the initial water density in graphene nanochannels with height H were compared. In both approaches, graphene spacer sheets were not included but channel heights were chosen to match those with $n = 1 – 6$ spacers. In each case the channel walls consisted of four stacked graphene sheets and had the atomistic hexagonal lattice structure of graphene and graphene sheets were held rigid throughout.

In the first approach (**Figure S1a**), a channel model with dimensions of $L_x = 30$ nm, $L_y = 10$ nm was constructed. Explicit water reservoirs were placed in direct contact with both ends of the channel in the x-direction, which in turn were placed in contact with a vacuum region. 100 ns canonical MD simulations were performed, during which time a dynamic equilibrium was established between water in the nanochannel and the reservoir. The interface between the liquid water reservoir and the vacuum region moved during the simulation, ensuring that the water in the reservoir maintained the correct density even as water molecules moved from the reservoir to the nanochannel. The density was calculated using the number of water molecules residing in the channel at the end of the 100 ns simulation. The other details of this MD simulation are the same as described as in **Section 1** above.

In the second approach (**Figure S1b**), a fully periodic channel model was filled with water using Grand Canonical Monte Carlo (GCMC) simulations. Due to the higher relative computational cost of this class of simulation, smaller graphene sheets ($L_x = 3.4$ nm, $L_y = 3.4$ nm) were used, and the density was only calculated for channel heights corresponding to the $n = 1 – 4$ systems. In the GCMC approach, water in the channel established an equilibrium with a hypothetical reservoir at fixed chemical potential *via* molecule insertion/deletion trial moves. Water molecules in the channel were also subjected to MC translation and rotation trial moves. Water molecule rotation, translation and insertion/deletion moves were chosen randomly using probabilities of 0.25, 0.25 and 0.5, respectively. The chemical potential, which determines the acceptance probability of water molecule insertion/deletion moves, was set to –43.1 kJ mol^{-1}. This value was found to reproduce the correct density of bulk liquid water at 298 K and 0.1 MPa in a separate simulation of bulk water. At equilibrium, achieved between 9.0×10^6 and 1.8×10^6 steps depending on the channel height, the average number of water molecules in the channel converged. The final density was obtained from the average number of water molecules in the channel over 6×10^6 MC steps. This simulation methodology follows a commonly employed procedure described elsewhere. [10]

Table S1 compares the area densities, ρ_{2D}, obtained using the two independent methodologies. The densities obtained using MD simulations were chosen as input for the nanochannel simulations described in detail in the main text. Both approaches result in very similar densities reinforcing the robustness of the initial density values chosen for the hydrated graphene nanochannel models. Water was added to the graphene nanochannel models using this target density and the Gromacs “gmx solvate” tool.

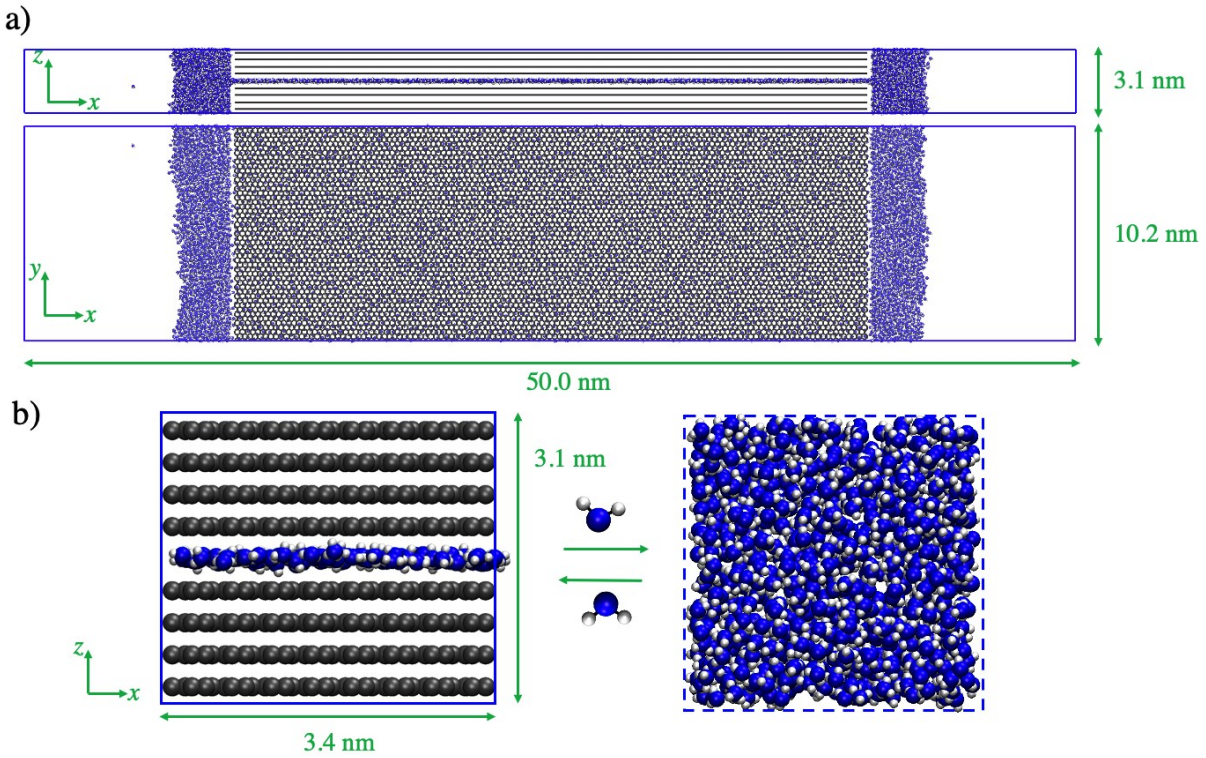

Figure S1. a) MD and b) GCMC simulation setups employed to obtain initial water densities. Carbon atoms are represented by black spheres or lines and water molecules are represented by blue and white spheres. The blue dashed line in b) represents a hypothetical liquid water reservoir that is not explicitly simulated.

Tables S1. Final area densities, ρ_{2D}, obtained from two the separate simulation setups based on MD and MC simulations that are shown in **Figure S1**.

n	**ρ_{2D} (molecules nm^{-2})**	
	MD	**GCMC**
1	11.0	11.0
2	21.5	22.0
3	33.8	34.3
4	44.4	46.2
5	55.6	-
6	67.3	-

3. Cut-Off Sensitivity

Using the initial non-bonded cut-off radius, r_{cut} = 1.2 nm, the dry n = 1 nanochannel collapsed with graphite slabs bending to close the nanochannel. In contrast, dry nanochannels with n > 1 were stable, i.e. the peak position in the nanochannel height distribution $P(H)$ was approximately equal to its initial value. However, whether the dry nanochannels collapsed or not was found to be strongly dependent on the choice of r_{cut}. Upon performing several simulations with gradually increasing r_{cut} up to 2.6 nm, nanocapillaries with n > 1 successively collapsed. Using r_{cut} = 2.0 nm, nanochannel collapse was observed for n = 4. However, the n = 5 and n = 6 nanochannels were stable and did not collapse for any cut-off radius. The strong cut-off dependence for small n can be explained by consideration of the large potential energy of interaction between a pair of graphene sheets. For example, the n = 4 nanochannel collapses to 0.34 nm from its initial height of 1.7 nm. Although at r_{ij} = 1.7 nm the vdW interaction energy between a pair of carbon atoms calculated from **Equation S1** is only −0.0001 kJ mol^{-1}, the

interaction energy between a pair of graphene sheets separated by 1.7 nm is −164 kJ mol^{-1}. Summed over all carbon atoms and all graphene sheets the vdW attraction between two graphite slabs at 1.7 nm is not negligible, explaining the sensitivity to r_{cut}. A 2.0 nm cut-off was used for the remainder of the results presented in this study. It was separately confirmed that increasing the cut-off from 1.2 nm to 2.0 nm did not result in any differences in the simulated properties of bulk TIP4P2005 water.

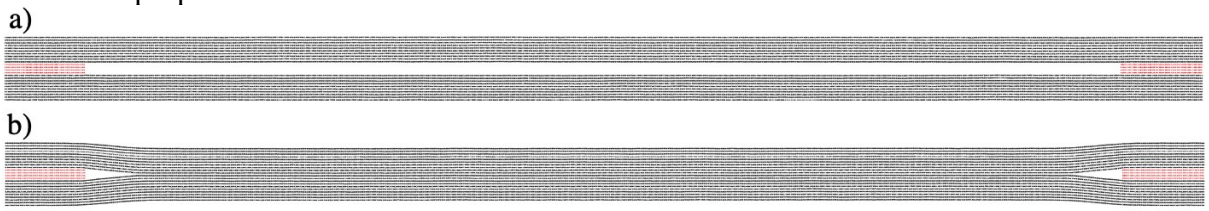

Figure S2. Comparison of dry n = 4 nanochannel collapse using a) r_{cut} = 1.2 nm and b) r_{cut} = 2.0 nm.

4. Calculation of Graphite-Water Potential

The profile of total potential energy felt by a water molecule due to the graphite walls, $V_{gw}(z)$, used to calculate the hydration pressure in **Equation 2** of the main text, was computed from

$$V_{gw}(z) = u_{gw}(z) + u_{gw}(H - z) \quad \text{(S2)}$$

where $u_{gw}(z)$ is the potential due to the bottom graphite slab and $u_{gw}(H - z)$ is the potential due to the top graphite slab. Approximating the slabs as infinite and structureless in the xy-plane means $u_{gw}(z)$ in **Equation S2** can be calculated from the integrated form of the Lennard-Jones 12-6 potential, the 10-4-3 (Steele) potential[10-12]

$$u_{gw}(z) = 2\pi\rho_c\Delta\varepsilon_{co}\sigma_{co}^2\left[\frac{2}{5}\left(\frac{\sigma_{co}}{z}\right)^{10} - \left(\frac{\sigma_{co}}{z}\right)^4 - \left(\frac{{\sigma_{co}}^4}{3\Delta(z + 0.61\Delta)^3}\right)\right] \quad \text{(S3)}$$

where ρ_C is the number density of carbon atoms in graphite (114 nm^{-3}) and Δ is the spacing between graphene layers in the graphite slab (0.34 nm).

5. Comparison of Properties Obtained with Flexible and Rigid Graphene Sheets

In the main text the water diffusion coefficient and hydration pressure were calculated (**Figure 5**) using the initial nanochannel height, H_{init}, and final nanochannel height after simulation relaxation, H_{final}, demonstrating some significant differences in water diffusion and hydration pressure especially at small n. **Figure S3** also compares the density profiles, $\rho_O(z)$, obtained using initial and final nanochannel heights. The largest difference in $\rho_O(z)$ between initial and relaxed systems was observed for the n = 2 system, due to the significant change in nanochannel height upon relaxation.

For n = 1, no differences were observed in $g_{2D}(r)$ and $P(\theta)$ between flexible and rigid nanochannel models, irrespective of whether the nanochannel height takes the initial (H_{init} = 0.68 nm) or equilibrated (H_{final} = 0.66 nm) value in the rigid case. For n = 2 nanochannels, both rigid and flexible $g_{3D}(r)$ and $g_{2D}(r)$ were identical when the equilibrated channel height (H_{final} = 0.94 nm) was used. On the other hand, using the initial channel height (H_{init} = 1.02 nm), slight differences in the structure of water were observed. For example, a less intense first maximum in both $g_{2D}(r)$ / $g_{3D}(r)$ and a shifted position of the second maximum in $g_{3D}(r)$. Regarding the effect of flexibility on the dynamics of confined water, the flexible model diffusion coefficients were somewhat lower than the rigid case using the initial H for n = 1 and n = 2. However, agreement was significantly improved using H_{final} for the rigid model instead. In general, the properties of confined water obtained directly from simulations with flexible graphite slabs were extremely similar to those obtained from simulations with rigid graphite slabs with H_{final}. This means that, providing that the rigid model nanochannel height matches the equilibrated

value from the flexible simulations (H_{final}), the approximation of rigid, non-interacting sheets is reasonable, and they can be employed to accurately predict the properties of confined water.

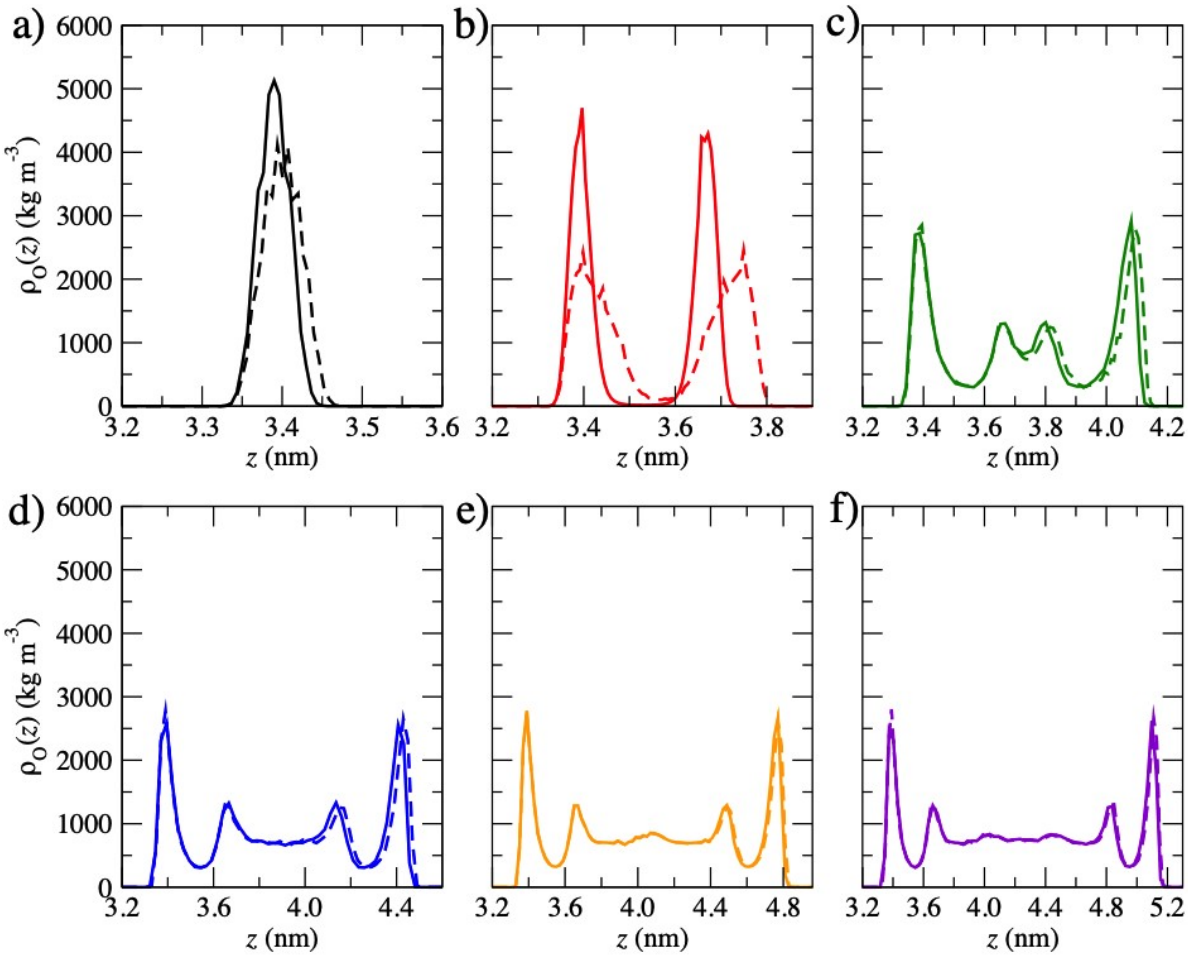

Figure S3. Oxygen density profiles, $\rho_O(z)$, across the nanochannel height for n = 1 (a) – 6 (f) for flexible model (solid lines) and rigid models using H_{init} (dashed lines).

6. Effect of Graphite Slab Thickness

Additional simulations were performed with a larger number of graphene sheets in the graphite slabs, to establish if the stability of the simulated nanochannels was dependent on the slab thickness. This was deemed necessary because the thickness of the graphite slabs in the real device (~100 nm) [13] is greater than is reasonably computationally accessible to the present simulations. Simulations using graphite slabs containing double the number of graphene sheets (20 nm) resulted in the same $P(H)$ and final nanochannel height for every model. For the dry models, n = 1 – 4 nanochannels collapsed but n = 5 – 6 did not collapse. This is the same as the result obtained with a thinner slab containing 10 sheets. For the hydrated models, the hydration pressure of the n = 1 model was also calculated, resulting in a hydration pressure of –22 MPa, in good agreement with the value obtained using thinner graphite slabs (–25 MPa).

7. Properties of Bulk Water

Additional MD simulations were performed to benchmark the properties of bulk liquid TIP4P/2005 water for comparison purposes. **Figure S4a** shows the three-dimensional oxygen-oxygen radial distribution function, $g_{3D}(r)$ and its integral, $n_{3D}(r)$, which can be used to obtain coordination numbers. $g_{3D}(r)$ displays a series of smoothly oscillating peaks and troughs with intensities tending towards 1 with increasing r, which is a manifestation of the continuous

breaking and reformation of hydrogen bonds render a disorder network. The first peak corresponds to the nearest neighbour atoms and is positioned at 0.278 nm, in good agreement with the experimental value of 0.281 nm.[14] The average number of neighbour oxygen atoms can be estimated from $n_{3D}(r)$ using a value of r which captures the first peak in $g_{3D}(r)$. In bulk TIP4P/2005, $n(r) = 4.0$ at $r = 0.32$ nm.

Figure S4b shows the mean-squared displacement (MSD) of water in the region between 0 and 100 ps. The linearly increasing MSD with respect to time, t, is indicative of liquid-like behaviour. The MSD can be used to compute the water translation self-diffusion coefficient, D, via the Einstein relation

$$D = \frac{1}{2dt}\lim_{t\to\infty}\left\langle |r_{i,d}(t) - r_{i,d}(0)|^2 \right\rangle \quad \text{(S4)}$$

where d is the dimensionality. Diffusion coefficients in periodic MD simulations are known to be sensitive to finite-size effects, with a mobility that increases with simulation cell length. [15, 16] **Figure 4c** shows the change in the diffusion coefficient of water with respect to inverse simulation cell length, L. The diffusion coefficient was corrected for finite size effects by linear extrapolation of D with respect to $1/L$ to infinite box size ($1/L = 0$). The resulting diffusion coefficient is 2.4×10^{-5} cm^2 s^{-1}, in good agreement with experimental value of 2.3×10^{-5} cm^2 s^{-1}. [17] The diffusion coefficient calculated for the smallest simulation, $1/L = 0.4$ nm^{-1}, is 2.1×10^{-5} cm^2 s^{-1}, in agreement with the original TIP4P/2005 parameterisation study in which a similar box size was employed.[1]

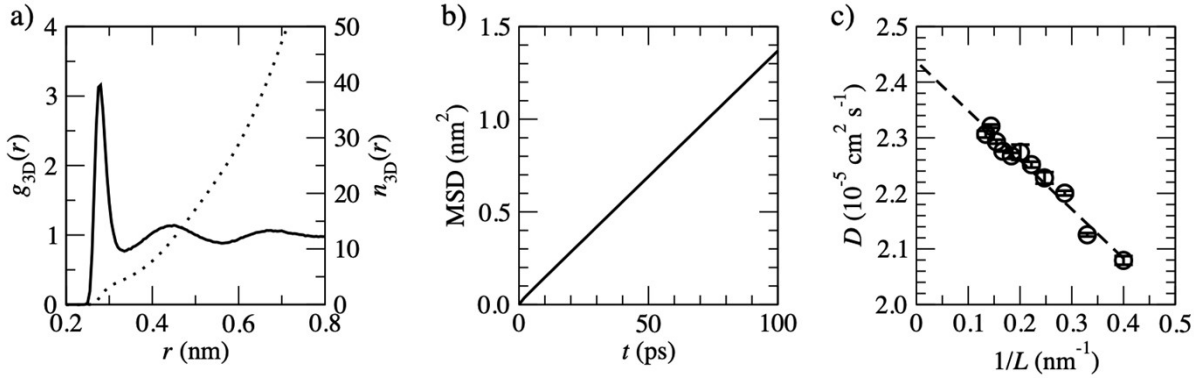

Figure S4. Properties of bulk TIP4P/2005 at 298 K and 1 bar. a) radial distribution function, $g_{3D}(r)$, and coordination number, $n_{3D}(r)$, for oxygen-oxygen pairs shown with solid and dotted line, respectively. b) mean squared displacement of water molecules up to $t = 100$ ps. c) water diffusion coefficients, D, plotted against the reciprocal of simulation cell side length, L. The dashed line is a linear fit.

8. Angle distributions

Since the oxygen-oxygen-oxygen angle distributions, $P(\theta)$, such as the one shown in **Figure 6b** of the main text, are dependent on the choice of neighbour cut-off, the sensitivity of $P(\theta)$ with respect to cut-off was calculated and the result for the flexible $n = 1$ model is shown in **Figure S5**. Various neighbour cut-offs were chosen based on distances corresponding to the features in $g_{2D}(r)$. Starting with a cut-off of 0.28 nm, which is the position of the first maximum in $g_{2D}(r)$ and includes only the nearest neighbours (1.3 on average), only a single peak in $P(\theta)$ was observed at 103°, close to the expected angle for a system with tetrahedral symmetry/coordination. Extending the cut-off to 0.32 nm, captures most of the area under the first peak in $g_{2D}(r)$ and includes an average of 3.2 oxygen neighbours. Using this cut-off, $P(\theta)$ becomes broader, with an additional peak and shoulder feature at 177° and 58°, respectively. The additional peak at 177° corresponds to nearly co-linear chains of three oxygen atoms and

the shoulder at 58° corresponds to the angle between first and second nearest neighbours in a hydrogen-bonded ring. Extending further the cut-off to 0.36 nm, which corresponds to the position of the first minimum in $g_{2D}(r)$, the shoulder feature intensifies to a significant peak and shifts to smaller θ. The peak continues to shift and intensify as the cut-off is further increased to the position of the second maximum in $g_{2D}(r)$ (0.46 nm), the position of the second minimum in $g_{2D}(r)$ (0.50 nm) and the position of the third maximum in $g_{2D}(r)$ (0.56 nm). The third maximum in $g_{2D}(r)$ at 0.56 nm is not present in the bulk water $g_{3D}(r)$ so is a confinement effect. The non-zero $P(\theta)$ for the 0.56 nm cut-off for $\theta = 0 - 30°$ suggests that the third maximum in $g_{2D}(r)$ can be attributed to the angle formed by first and second nearest neighbours along nearly linear chains, which are present under confinement in the $n = 1$ channel but not in bulk water.

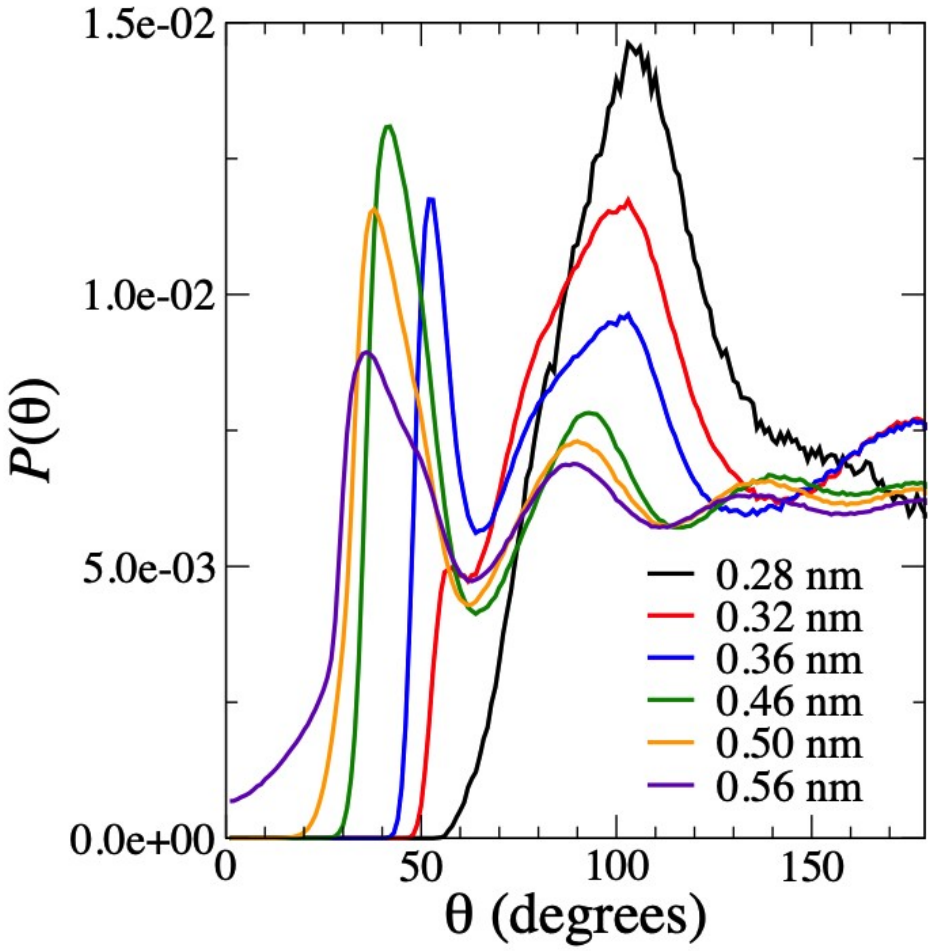

Figure S5. Dependence of two-dimensional O-O-O angle distributions, $P(\theta)$, on the nearest neighbour cut-off using cut-offs of 0.28, 0.32, 0.36, 0.46, 0.50 and 0.56 nm for the flexible $n = 1$ nanochannel model.

9. Dependence of Confined Water Properties on Nanochannel Height

Figure 6a of the main text shows the two-dimensional oxygen-oxygen radial distributional function, $g_{2D}(r)$, for the flexible $n = 1$ nanochannel which contains a water monolayer. The three-dimensional oxygen-oxygen radial distribution functions, $g_{3D}(r)$, were also calculated for all nanochannel heights and these are shown in **Figure S6a**. For $n = 1$, the first peak in $g_{3D}(r)$ is at the same distance as $g_{2D}(r)$ (0.28 nm) but has a higher intensity due to the spherical normalisation factor in $g_{3D}(r)$. The feature at $r = 0.56$ nm, which is due to linear chains of three oxygen atoms, can be seen in both $g_{2D}(r)$ and $g_{3D}(r)$. For $n > 2$, the intensity of the first peak in

$g_{3D}(r)$ gradually reduces because of the decreasing confinement. In addition, the peak at r = 0.56 nm disappears for $n > 2$ so can be considered unique to the n = 1 (monolayer water) nanochannel. For n = 2, $g_{3D}(r)$ displays a clear peak at 0.40 nm which is not present in the other systems and can be considered unique to the n = 2 (bilayer water) nanochannel. The average number of nearest neighbour oxygens (at the position of the first minimum in $g_{3D}(r)$) in the bilayer is 3.96, virtually the same as in the monolayer. This means the second maximum in $g_{3D}(r)$ for n = 2 can be attributed to interactions between oxygens in separate water layers which are shown to be well-defined in **Figure 4b**.

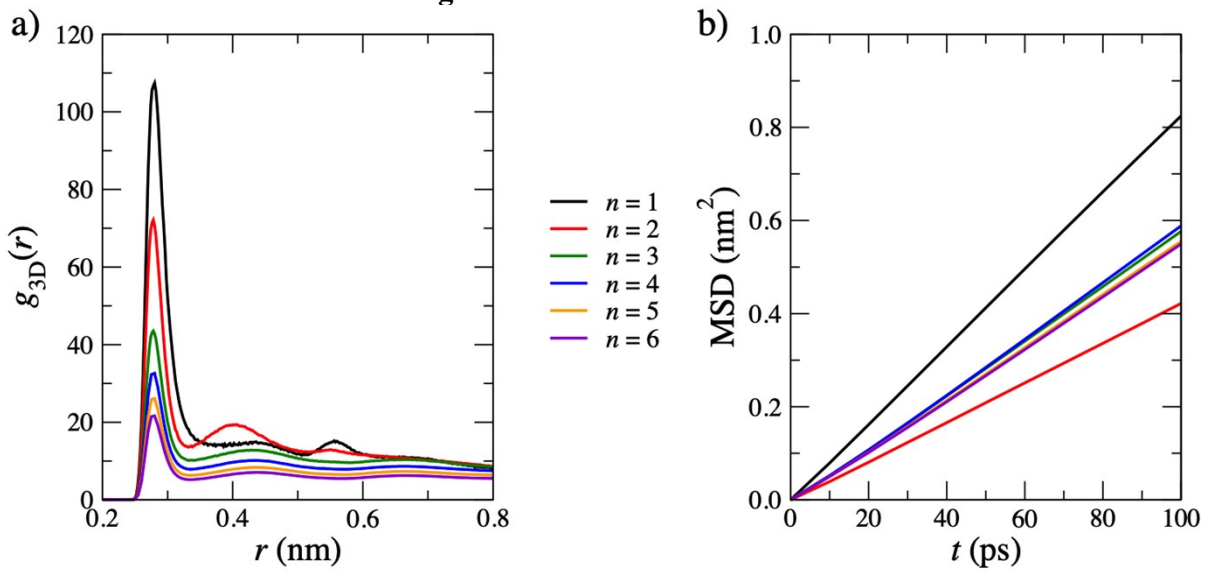

Figure S6. a) three-dimensional radial distribution function, $g_{3D}(r)$, for oxygen-oxygen atom pairs and b) mean-squared displacement (MSD) of water in the y-direction between t = 0 and 100 ps for n = 1 (black), n = 2 (red), n = 3 (green), n = 4 (blue), n = 5 (orange), n = 6 (purple) flexible nanochannel models.

Figure 6b shows the mean-squared displacement (MSD) in the flow (y) direction between 0 and 100 ps for all flexible nanochannel models. The slope of MSD with respect to time in the linear regime defines the corresponding diffusion coefficient in this dimension, D_y, *via* **Equation S4**. The fastest diffusion of water occurs for n = 1 and the slowest for n = 2, indicated by the slope of the MSD. For all other n the plots of MSD against time are virtually indistinguishable. The diffusion coefficients for all three dimensions shown in **Figure 5** of the main text are provided in **Table S2.** Diffusion coefficients in the x- and z-dimensions are not sensitive to finite-size effects because the nanochannel model dimensions exactly match those of the real experimental device we seek to replicate. However, the nanochannel is periodic in the y-dimension so the calculated diffusion coefficients may be subject to finite-size effects in this dimension. The approach adopted to correct for finite-size effects in bulk water in Section 7 above was not possible for the nanochannel models, due to limitations associated with computational cost. Therefore, the calculated diffusion coefficients in the flow direction are likely to be an underestimate compared to water in the real device.

Table S2. Diffusion coefficients ($\times 10^{-5}$ cm^2 s^{-1}) for flexible and rigid nanochannel models. The rigid data was calculated using the initial nanochannel height, H_{init}. Errors are less

than 0.3×10^{-5} cm^2 s^{-1}. Although calculated using Equation S4, diffusion coefficients in the *z*-direction are in the sub-diffusive regime.

n	**flexible**			**rigid (H_{init})**		
	x	***y***	***z***	***x***	***y***	***z***
1	3.0	4.0	0.0	3.4	4.9	0.0
2	1.2	2.0	0.0	1.7	3.0	0.1
3	2.1	2.9	0.4	2.0	2.8	0.5
4	2.2	2.9	0.7	2.3	2.9	0.7
5	2.2	2.8	0.9	2.1	2.7	1.0
6	2.2	2.8	1.1	2.1	2.7	1.1

10. Sensitivity of Water Properties to Intermolecular Potential

In this section we assess the sensitivity of the results to the choice of intermolecular potential. For the $n = 1$ system, three additional simulations of the hydrated, flexible nanochannels were performed using several other intermolecular potentials commonly employed for graphene-water systems in the literature. In the first, the SPC/E water model[18] and the carbon-oxygen cross parameter set 24 of Werder *et al* (ε_{CO} = 0.4785 kJ mol^{-1}, σ_{CO} = 0.3275 nm) were employed (Werder24 / SPC/E). [19] Secondly, the SPCE water model and cross parameter set 28 of Werder *et al* (ε_{CO} = 0.3920 kJ mol^{-1}, σ_{CO} = 0.3190 nm) were employed (Werder28 / SPC/E). [19] Finally, following the examples of Zhu *et al.* [20] and Algara-Siller *et al.*[21], cross parameter set 28 of Werder *et al* was mixed with the TIP4P/2005 water model (Werder28 / TIP4P/2005).

For the two simulations employing the SPC/E model, water spontaneously entered the nanochannels in the MD channel filling simulations. However, the final densities obtained were ~13% higher (ρ_{2D} = 12.5 nm^{-2}) than those obtained using the TIP4P/2005 model. These densities are very close to the maximum value for a water monolayer (12.3 nm^{-2}) reported by Pestana *et al.*, [22] who systematically varied the initial density of confined water using the SPC/E model. The densities obtained using the SPC/E water model were independent of whether the employed cross-parameters ε_{CO} and σ_{CO} model a hydrophobic (water contact angle on graphite of 95° using Werder28) or hydrophilic surface (water contact angle on graphite of 65° using Werder24). [19] The nanochannel height peak in $P(H)$ using SPC/E water was positioned at 0.65 nm, very similar to the peak position obtained using TIP4P/2005. In addition, a hydration pressure, p_{hyd}(H), of −16 MPa was obtained, slightly less negative than the equivalent value obtained using TIP4P/2005 (−25 MPa).

Figure S7 compares the properties of the water monolayer obtained using the Amber / TIP4P/2005 and Werder28 / SPC/E potentials. Although the oxygen density profiles $\rho_O(z)$ appear very similar (**Figure S7a**) there are qualitative differences in the in-plane structure of water. Using the SPC/E model significant in-plane ordering was observed, as shown by the intense peaks and troughs in $g_{2D}(r)$ beyond the first maximum (**Figure S7b**) and a deep minimum was observed at 0.50 nm, which corresponds to 7.9 neighbouring oxygen atoms. The second maximum in $g_{2D}(r)$ at 0.57 nm, due to next-but-one neighbours along linear chains of oxygen atoms, is significantly more intense using the SPC/E model. $P(\theta)$ (**Figure S7c**) further confirms the in-plane order with two clearly defined peaks at 90° and 162°. The first peak has symmetrical shoulder features at 74° and 106° which corresponds to three distinct O-O-O angles. The 90° peak indicates regions with square symmetry and the 74° and 106° shoulders, which sum to 180°, indicate regions of rhombic symmetry. The second peak at 162° corresponds to the nearly linear chains of oxygen atoms. The simulation snapshot in **Figure**

S7fii shows that this is due to the formation of an ordered structure with square/rhombic symmetry, which is not evident from the equivalent snapshot of TIP4P/2005 water in **Figure S7fi**. Finally, the MSD shown in **Figure S7d** shows that the mobility of monolayer water is very low using the SPC/E model compared to bulk water. Diffusion in the flow direction was an order of magnitude lower (D_y = 0.4 × 10^{-5} cm^2 s^{-1}) than the result using the TIP4P/2005 model. The properties of SPC/E water obtained using Werder24 cross-parameters are the same as those using Werder28 despite predicting significantly different contact angles for a water droplet on graphite (65° *vs* 95° for Werder24 *vs* Werder28, respectively). [19] It can therefore be concluded that the primary reason for the significantly different water properties highlighted in **Figure S7** are due to the water model employed and not the carbon-oxygen cross interaction parameters used in the intermolecular potential.

For the mixed parameter set employed in Algara-Sillar *et al.* [21] and Zhu *et al*. [20] (Werder28 / TIP4P/2005), water did not enter the channel over the course of either the MD or MC channel filling simulations. Since no water entered the n = 1 nanochannel using these parameters, water was manually added using the density obtained using the Amber / TIP4P/2005 potential combination instead. In the rigid nanochannel a disordered monolayer with mobile water molecules was obtained. However, in the flexible nanochannel the water monolayer was found to be unstable using this intermolecular potential, as shown in **Figure S8b**, whereby the outer regions of the nanochannel collapsed and a non-planar 'bubble' of water formed in the centre of the nanochannel. The channel height distribution, $P(H)$, in **Figure S8a** shows peaks at H = 0.34 nm, 0.68 nm and 1.75 nm. These peaks correspond to the collapsed region, spacer region and the centre of the bubble regions, respectively. $P(H)$ does not equal zero between the peaks due to the gradual increase in channel height from the edge to the centred of the bubble. This monolayer instability is perhaps unsurprising since, using this potential, water did not enter during the channel filling simulations. This is qualitatively different behaviour to that of Algara-Sillar *et al.*, [21] who instead reported a rhombic-ice monolayer using the same intermolecular potential. The result emphasizes the important consideration of potential transferability. The mixing of cross-parameters developed for use with a specific water model (SPC/E) with a different model (TIP4P/2005) should be avoided, due to the interdependency of graphite-water and water-water interactions in the intermolecular potential.

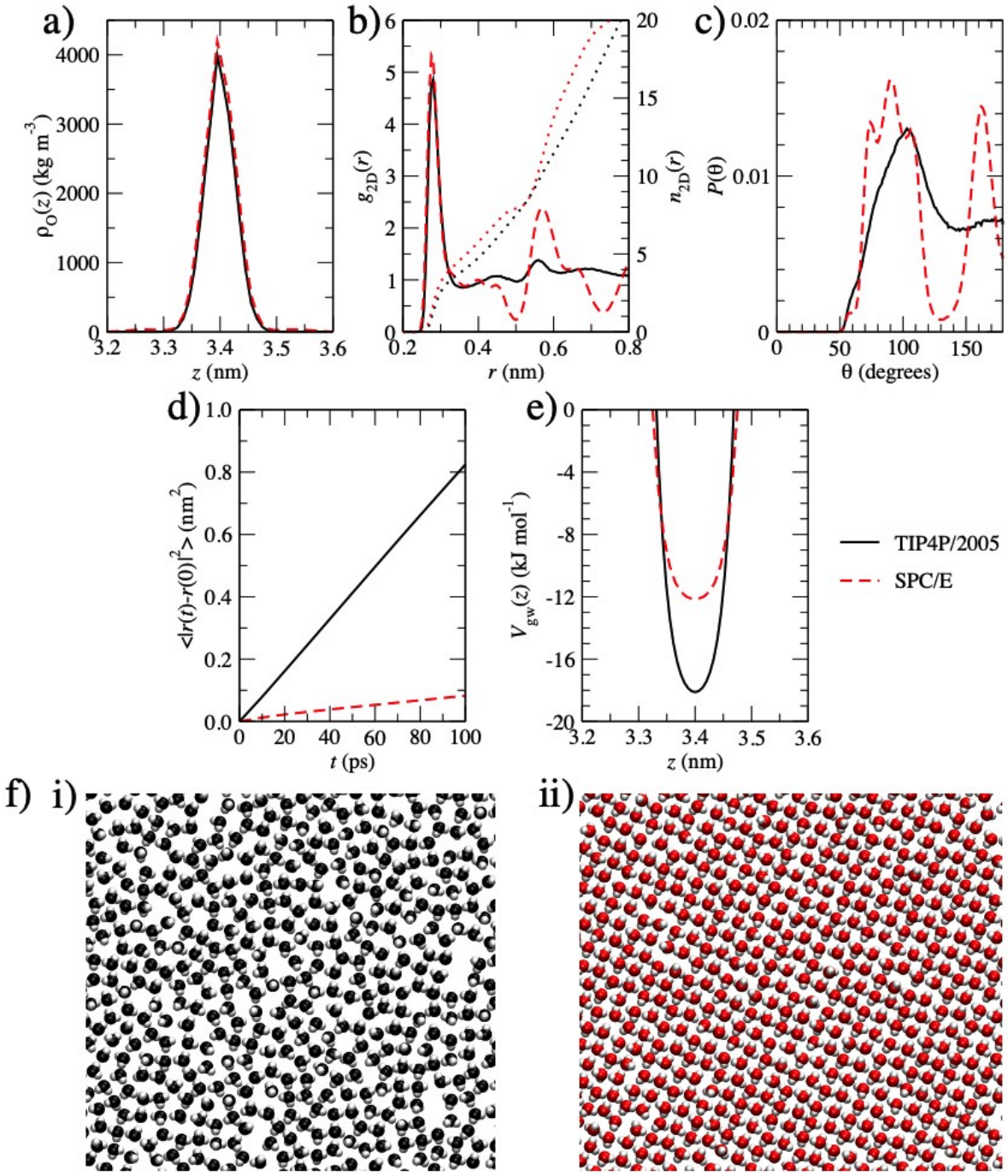

Figure S7. Comparison of monolayer water properties in flexible n = 1 nanochannels between the Amber / TIP4P/2005 potential (black lines) and the Werder28 / SPC/E potential (red, dashed lines) including a) density profile, $\rho_O(z)$, b) two-dimensional O-O radial distribution function, $g_{2D}(r)$, and its integral, $n_{2D}(r)$ (dotted lines), c) in-plane O-O-O angle distributions, $P(\theta)$, using a neighbour cut-off of 0.28 nm, d) MSD of water in the y-dimension, e) total graphite-water potential energy across the nanochannel height and f) representative simulation snapshots of the monolayer obtained using the i) Amber / TIP4P2005 potential and ii) Werder28 / SPCE potential.

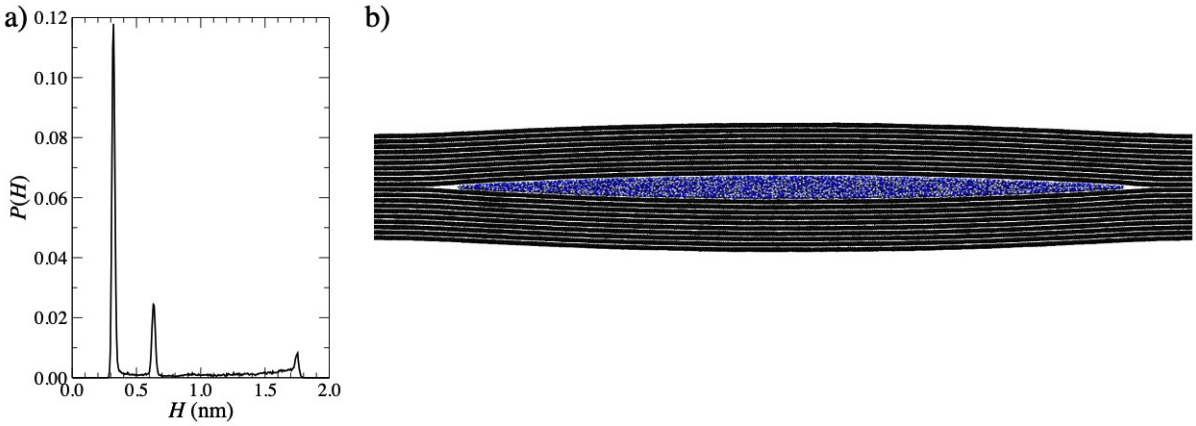

Figure S8. a) interlayer distance distribution, $P(H)$, and b) representative simulation snapshot of the central region of the flexible n = 1 nanochannel using the Werder28 / TIP4P/2005 potential.

References

1. Abascal, J.L.F. and C. Vega, *A general purpose model for the condensed phases of water: TIP4P/2005.* Journal of Chemical Physics, 2005. **123**(23): p. 234505.
2. Cornell, W.D., et al., *A second generation force field for the simulation of proteins, nucleic acids, and organic molecules (vol 117, pg 5179, 1995).* Journal of the American Chemical Society, 1996. **118**(9): p. 2309-2309.
3. Williams, C.D., P. Carbone, and F.R. Siperstein, *Computational Characterisation of Dried and Hydrated Graphene Oxide Membranes.* Nanoscale, 2018. **10**: p. 1946-1956.
4. Pall, S. and B. Hess, *A flexible algorithm for calculating pair interactions on SIMD architectures.* Computer Physics Communications, 2013. **184**(12): p. 2641-2650.
5. Nose, S., *A Molecular Dynamics Method for Simulations in the Canonical Ensemble.* Mol. Phys., 1984. **52**(2): p. 255-268.
6. Hoover, W.G., *Canonical Dynamics: Equilibrium Phase-Space Distributions.* Physical Review A, 1985. **31**(3): p. 1695-1697.
7. Miyamoto, S. and P.A. Kollman, *Settle: an Analytical Version of the SHAKE and RATTLE Algorithm for Rigid Water Models.* J. Comput. Chem., 1992. **13**(8): p. 952-962.
8. Essmann, U., et al., *A Smooth Particle Mesh Ewald Method.* Journal of Chemical Physics, 1995. **103**(19): p. 8577-8593.
9. Van der Spoel, D., et al., *GROMACS: Fast, Flexible, and Free.* Journal of Computational Chemistry, 2005. **26**(16): p. 1701-1718.
10. Striolo, A., et al., *Water adsorption in carbon-slit nanopores.* Langmuir, 2003. **19**(20): p. 8583-8591.
11. Steele, W.A., *The Physical Interaction of Gases with Crystaline Solids. I Gas-Solid Energies and Properties of Isolated Adsorbed Atoms.* Surface Science, 1973. **36**: p. 317-352.
12. Balbuena, P.B. and K.E. Gubbins, *Theoretical Interpretation of Adsorption Behavior of Simple Fluids in Slit Pores.* Langmuir, 1993. **9**(7): p. 1801-1814.
13. Radha, B., et al., *Molecular transport through capillaries made with atomic-scale precision.* Nature, 2016. **538**(7624): p. 222-225.
14. Bergmann, U., et al., *Nearest-neighbor oxygen distances in liquid water and ice observed by x-ray Raman based extended x-ray absorption fine structure.* Journal of Chemical Physics, 2007. **127**(17).

15. Yeh, I.C. and G. Hummer, *System-size dependence of diffusion coefficients and viscosities from molecular dynamics simulations with periodic boundary conditions.* Journal of Physical Chemistry B, 2004. **108**(40): p. 15873-15879.
16. Williams, C.D., et al., *The Development of a Classical Force Field To Determine the Selectivity of an Aqueous Fe3+-EDA Complex for TcO4- and SO42.* Journal of Chemical Theory and Computation, 2014. **10**(8): p. 3345-3353.
17. Mills, R., *Self-diffusion in Normal and Heavy-Water in Range 1-45 Degrees.* Journal of Physical Chemistry, 1973. **77**(5): p. 685-688.
18. Berendsen, H.J.C., J.R. Grigera, and T.P. Straatsma, *The missing term in effective pair potentials.* Journal of Physical Chemistry, 1987. **91**(24): p. 6269-6271.
19. Werder, T., et al., *On the water-carbon interaction for use in molecular dynamics simulations of graphite and carbon nanotubes.* Journal of Physical Chemistry B, 2003. **107**(6): p. 1345-1352.
20. Zhu, Y.B., et al., *Compression Limit of Two-Dimensional Water Constrained in Graphene Nanocapillaries.* Acs Nano, 2015. **9**(12): p. 12197-12204.
21. Algara-Siller, G., et al., *Square ice in graphene nanocapillaries.* Nature, 2015. **519**(7544): p. 443-445.
22. Pestana, L.R., L.E. Felberg, and T. Head-Gordon, *Coexistence of Multilayered Phases of Confined Water: The Importance of Flexible Confining Surfaces.* Acs Nano, 2018. **12**(1): p. 448-454.